A model for the compositions of non-stoichiometric intermediate phases formed by diffusion reactions, and its application to Nb_3Sn superconductors

X. Xu*, M. D. Sumption

Department of Materials Science and Engineering, the Ohio State University, Columbus, OH 43210 USA

*Electronic mail: xu.452@osu.edu

In this work we explore the compositions of non-stoichiometric intermediate phases formed by diffusion reactions: a mathematical framework is developed and tested against the specific case of Nb_3Sn superconductors. In the first part, the governing equations for the bulk diffusion and inter-phase interface reactions during the growth of a compound are derived, numerical solutions to which give both the composition profile and growth rate of the compound layer. The analytic solutions are obtained with certain approximations made. In the second part, we explain an effect that the composition characteristics of compounds can be quite different depending on whether it is the bulk diffusion or grain boundary diffusion that dominates in the compounds, and that "frozen" bulk diffusion leads to unique composition characteristics quite distinct from equilibrium expectations; then the model is modified for the case of grain boundary diffusion. Finally, we apply this model to the Nb_3Sn superconductors and propose the approaches to control their compositions.

Keywords: Non-stoichiometric compounds, diffusion reaction, composition, model, Nb_3Sn

Introduction

Intermediate phases with finite composition ranges represent a large class of materials, and their compositions may influence their performance in application, as demonstrated in a variety of materials, such as electrical conductivity of oxides (e.g., TiO_{2-y} [1]), electromagnetic properties of superconductors (e.g., Nb_3Sn and $YBa_2Cu_3O_{7-y}$ [2]), and mechanical properties of some

intermetallics (e.g., Ni-$Al_{0.4\text{-}0.55}$ [3]), etc. For instance, the superconducting Nb_3Sn phase, which finds significant applications in the construction of 12-20 T magnets[4,5], has a composition range of ~17-26 Sn at.%[6,7], and its superconducting transition temperature and magnetic field decrease dramatically as Sn content drops[4,7-8]. The Nb_3Sn phase, which is generally fabricated from Cu-Sn and Nb precursors through reactive diffusion processes, is always found to be Sn-poor (e.g., 21-24 at.%[4,8-9]), making composition control one of the primary concerns in Nb_3Sn development since 1970s[10]. Although a large number of previous experiments (e.g., [4,8-11]) have uncovered some factors that influence the Sn content, it is still a puzzle what fundamentally determines the Nb_3Sn composition. This work aims to fill that gap. Here it is worth mentioning that the composition interval of a compound layer does not necessarily coincide with its equilibrium phase field ranges – the former can be narrower (e.g., the Nb_3Sn example above) if the inter-phase interface reaction rates are slow relative to the diffusion rate across the compound, which results in discontinuities in chemical potentials at the interfaces.

There have been numerous studies regarding diffusion reaction processes, most of which have focused on layer growth kinetics (e.g.,[12-16]), compound formation and instability (e.g.,[14-16]), phase diagram determination (e.g.,[17]), and interdiffusion coefficient measurement (e.g.,[18]), while a systematic model exploring how to control compound composition is still lacking. We find it indeed possible to modify the model developed by Gosele and Tu[13] for deriving the layer growth kinetics of compounds to calculate their compositions; however, certain assumptions (e.g., steady-state diffusion and first-order interface reaction rates) that the model was based on may limit the accuracy of the composition results. In this work, we aim to develop a rigorous, systematic mathematical framework for the compositions of intermediate phases.

Results

Let us consider that an A_nB compound with a B content range of X_l - X_u ($X_l < X_u < 1$) is formed in a system of M-B/A, where M is a third element that does not dissolve in A_nB lattice[19], and the solubility of B in A is negligible[6]. This is the case we see for the Nb_3Sn example above (for which A stands for Nb, B for Sn, and M for Cu), but the work below can be modified for other cases. An isothermal cross section of such an M-A-B phase diagram at a certain temperature is shown in Fig. 1. The use of the third element M is to decrease the chemical potential of B, so that unwanted high-B A-B compounds (e.g., $NbSn_2$ and Nb_6Sn_5 [6]) that would form in the B/A binary system can be avoided. Similar to the Cu-Nb-Sn system, let us assume B is the primary diffusing species in the A_nB layer[20] and that the diffusivity of B in M-B is high[10]. A schematic of the M-B/A_nB/A system for a planar geometry is shown in Fig. 2, but the model can be modified for cylindrical and spherical geometries. Let us denote the M-B/A_nB and A_nB/A inter-phase interfaces as I and II, respectively, and the concentrations, chemical potentials, activities, and diffusion fluxes of B in the A_nB layers near interfaces I and II as X_I, μ_I, a_I, J_I, and X_{II}, μ_{II}, a_{II}, J_{II}, respectively. Let us also denote the X_Bs, μ_Bs, a_Bs of M-B source and A-X_l B as X_s, μ_s, a_s, and X_l, μ_l, a_l, respectively.

In this work let us assume the diffusivity of B in A_nB, D, and the molar volume of A_nB, V_m, do not vary with X_B, in which case the continuity equation in the A_nB layer is given by:

$$\frac{\partial X_B}{\partial t} = D\frac{\partial^2 X_B}{\partial x^2} \tag{1}$$

According to mass conservation, in a unit time the amount of B transferring across the interface I should equal to that diffusing into A_nB from the interface I, and the amount arriving at the interface II should equal to that transferring across it, i.e., $dn/dt|_{\mathrm{I}} = J_I \cdot A_I$, and $dn/dt|_{\mathrm{II}} = J_{II} \cdot A_{II}$, where A_I and A_{II} are the areas of the interfaces I and II, respectively. The molar transport rate dn/dt across an interface equals to $r \cdot A_{int} \cdot \exp(-Q/RT) \cdot [1-\exp(-\Delta\mu/RT)]$, where r is the transfer rate

constant for this interface with the unit of mol/(m^2·s), A_{int} is the interface area, Q is the energy barrier, R is the gas constant, T is the temperature in K, and $\Delta\mu$ is the driving force for atom transfer. For the interface I, $\Delta\mu|_{\mathrm{I}} = \mu_s - \mu_I$. For the interface II, $\Delta\mu|_{\mathrm{II}} = \mu_{II} - \mu_l$, because $\mu_B(\mathrm{A}) = \mu_B(\mathrm{A}\text{-}X_l\ \mathrm{B})$. With $J_B = -(D/V_m)\cdot(\partial X_B/\partial x)$, we have:

$$r_I \exp\left(-\frac{Q_I}{RT}\right)\left[1-\exp\left(-\frac{\mu_s-\mu_I}{RT}\right)\right] = -\frac{D}{V_m}\frac{\partial X_B}{\partial x}\Big|_I \tag{2}$$

$$r_{II} \exp\left(-\frac{Q_{II}}{RT}\right)\left[1-\exp\left(-\frac{\mu_{II}-\mu_l}{RT}\right)\right] = -\frac{D}{V_m}\frac{\partial X_B}{\partial x}\Big|_{II} \tag{3}$$

Eqs. (2) and (3) are the boundary conditions for Eq. (1). Note that X_s drops with annealing time as B in M-B is used for A_nB growth, so μ_s drops with t:

$$\frac{d\mu_s}{dt} = \frac{d\mu_s}{dX_s}\frac{dX_s}{dt} = -\frac{d\mu_s}{dX_s}\frac{n_M}{\left(n_M + n_{B0} - \int_t dn/dt\big|_I\right)^2}\frac{dn}{dt}\Big|_I \tag{4}$$

where n_M and n_{B0} are the moles of M and B in the M-B precursor. For those systems without the third element, μ_s is constant, and Eq. (4) is not needed. In addition, since the B atoms diffusing to the interface II are used to form new A_nB layers, we have:

$$\frac{dl}{dt} = \frac{J_{II}V_m}{X_{II}} = -\frac{D}{X_{II}}\frac{\partial X_B}{\partial x}\Big|_{II} \tag{5}$$

Eqs. (1)-(5) are the governing equations for the system set up above, solutions to which give both the $X_B(x, t)$ and the $l(t)$ of a growing A_nB layer. It should be noted that for the systems with large volume expansion associated with transformation from A to A_nB, stress effects need to be considered[21].

To simplify Eqs. (2) and (3), we notice that $1-\exp[-(\mu_s-\mu_I)/RT] = 1-a_I/a_s$, since $\mu_s-\mu_I = RT\ln(a_s/a_I)$; similarly, $1-\exp[-(\mu_{II}-\mu_l)/RT] = 1-a_l/a_{II}$. Let us also denote $D/[V_m\cdot r_I\cdot\exp(-Q_I/RT)]$ as φ_I, and $D/[V_m\cdot r_{II}\cdot\exp(-Q_{II}/RT)]$ as φ_{II}: clearly φ_I and φ_{II} represent the ratios of diffusion rate over

interface reaction rates, and have a unit of meter. Then Eqs. (2) and (3) can be respectively written as:

$$1-\frac{a_I}{a_s}=-\varphi_I\left.\frac{\partial X_B}{\partial x}\right|_I \tag{6}$$

$$1-\frac{a_l}{a_{II}}=-\varphi_{II}\left.\frac{\partial X_B}{\partial x}\right|_{II} \tag{7}$$

For now, let us consider two extreme cases.

First, for the case that the interface reaction rates are much higher than the diffusion rate across the A_nB layer (i.e., diffusion-rate limited), φ_I and φ_{II} are near zero; according to Eqs. (2)-(3), μ_Bs are continuous at both interfaces. Suppose μ_s and the position of interface I, x_I, are both constant with time, then X_I is also constant, and the solutions to Eqs. (1) and (5) are respectively $X_B(x, t) = X_I-(X_I-X_l)\cdot\mathrm{erf}\{(x-x_I)/[2\sqrt{(Dt)}]\}/\mathrm{erf}(k/2)$ and $l=k\sqrt{(Dt)}$ for the A_nB layer, where k can be numerically solved from $k\cdot\exp(k^2/4)\cdot\mathrm{erf}(k/2) = 2/\sqrt{\pi}\cdot(X_I-X_l)/X_l$. For instance, for $X_I = 0.26$ and $X_l = 0.17$, k=0.953. On the other hand, if the interface reaction rates are much lower than the diffusion rate across A_nB (e.g., as the A_nB layer is thin), φ_I and φ_{II} are large; according to Eqs. (2)-(3), X_B and J_B are nearly constant in the entire A_nB layer. Thus, $(1-a_B/a_s)/\varphi_I = (1-a_l/a_B)/\varphi_{II}$, from which a_B can be calculated. Integration of Eq. (5) gives: $l \propto t$, and the pre-factor depends on the interface reaction rates.

For a general case between these two extremes, the equations can only be solved with the $\mu(X)$ relations of M-B and A_nB provided. Next, let us consider a compound with a narrow composition range, so that as a Taylor series expansion is performed around X_l for its $a(X_B)$ curve, high-rank terms can be neglected because $|X-X_l| \le (X_u-X_l)$ is small; that is, $a_X \approx a_l + \kappa(X-X_l)$, where κ is the linear coefficient of the $a(X)$ curve. Given the complex boundary conditions for Eq. (1), to obtain the analytic solutions we introduce a second approximation if the A_nB

composition range is narrow: the $X(x)$ profile of the A_nB layer is linear so that at a certain time J is constant with x, such that $-(\partial X_B/\partial x)|_I \approx -(\partial X_B/\partial x)|_{II} \approx (X_I-X_{II})/l$. With these two approximations, we can solve Eqs. (6)-(7) and obtain that:

$$a_{II} = \frac{\sqrt{(\varphi_I a_s + \kappa l - \varphi_{II} a_s)^2 + 4\varphi_{II} a_l (\varphi_I a_s + \kappa l)} - (\varphi_I a_s + \kappa l - \varphi_{II} a_s)}{2\varphi_{II}} = \frac{2a_l}{1-\eta+\sqrt{(1-\eta)^2 + 4\eta \, a_l / a_s}} \quad (8)$$

where $\eta=\varphi_{II}a_s/(\varphi_I a_s+\kappa l)$. Then a_I can be calculated from a_{II}, and X_I and X_{II} can be calculated from a_I and a_{II} using $X = X_l + (a_X - a_l)/\kappa$.

To verify the results, the equations are solved for a hypothetical system analytically and numerically, with and without the assumption that $X(x)$ is linear, respectively. The obtained composition profiles are shown in Fig. 3 (a). For simplicity, μ_s of the system is set as μ_B(A-X_u B) and is constant (for Nb_3Sn systems, this means that Nb_6Sn_5 serves as Sn source), and the other parameters are specified in the figure. The difference between the analytic and numerical solutions is <0.1%, showing that the approximation of linear $X(x)$ is good if the composition range is small (2 at.% in this case). The $l(t)$ result (where t is the annealing time after the incubation period) from the numerical calculations is shown in Fig. 3 (b). While the analytic $l(t)$ solution is complicated, some $l(t)$ relations with simple forms can be used as approximations. The most widely used $l(t)$ relation for the case of constant μ_s is $l=bt^m$, in which m=1 for reaction-rate limited and m=0.5 for diffusion-rate limited; however, a defect with this relation is that as l increases from zero, it may shift from reaction-rate limited to diffusion-rate limited, so m may vary with t. Here a new relation $l=q[\sqrt{(t+\tau)}-\sqrt{\tau}]$ (where q is a growth constant and τ is a characteristic time) is proposed. Such a relation is consistent with $l^2/v_1+l/v_2=t$ (where v_1 and v_2 are constants related to diffusion rate and interface reaction rates, respectively) proposed by previous studies[13,14]. This relation overcomes the above problem because as $t << \tau$, $l = [q/(2\tau)]\cdot t$

and as $t >> \tau$, $l=q\sqrt{t}$. As can be seen from Fig. 3 (b), a better fit to the numerical $l(t)$ curve in the whole range is achieved by $l=q(\sqrt{(t+\tau)}-\sqrt{\tau})$.

Discussion

Before discussing the application of this model to a specific material system, it must be pointed out that all of the analysis and calculations above are for the case that B diffuses through A_nB bulk. In such a case, for an M-B/A_nB/A system, as μ_s drops with the growth of A_nB layer, $X_B(x)$ of A_nB should decrease with μ_s, because $\mu_s \geq \mu_I \geq \mu_{II} \geq \mu_l$. Finally, one of two cases will occur: either μ_s drops to μ_l (if A is in excess) so the system ends up with the equilibrium among A, A-X_l B, and M-X_1 B (as shown by the shaded region in the isothermal M-A-B phase diagram in Fig. 1), or A is consumed up and A_nB gets homogenized with time and finally $\mu_B(A_nB)=\mu_B$(M-B) (as shown by the dashed line in Fig. 1). In either case, A_nB eventually reaches homogeneity.

However, we find that the composition could be different for a compound in which the bulk diffusion is low while grain boundary diffusion dominates. One such example is Nb_3Sn, the composition of which displays some extraordinary features. As an illustration, the X_{Sn}s of a Cu-Sn/Nb_3Sn/Nb diffusion reaction couple after various annealing times are shown in Fig. 4. Clearly, as the X_{Sn} (and μ_{Sn}) of Cu-Sn drop with time, the X_{Sn}s of Nb_3Sn do not drop accordingly; instead, they more or less remain constant with time. In addition, from 320 hours to 600 hours, although Nb has been fully consumed, the X_{Sn} of Nb_3Sn does not homogenize (i.e., the X_{Sn} gradient does not decrease) with time. In many other studies on Cu-Sn/Nb systems with Nb in excess (e.g., [4,8-9]), even after extended annealing times after the Nb_3Sn layers have finished growing (which indicates that the Sn sources have been depleted, i.e., μ_{Sn}s have dropped to μ_l), X_{Sn}s of Nb_3Sn remain high above X_l, without dropping with annealing time.

The reason for these peculiarities is that grain boundary diffusion in Nb_3Sn dominates due to extremely low bulk diffusivity (e.g., lower than 10^{-23} m^2/s at 650 °C)[20,22,23] and small Nb_3Sn grain size (~100 nm). In this case, our model and equilibrium-state analysis apply only to the diffusion zones (i.e., the grain boundaries and the inter-phase interfaces) instead of the bulk. To clarify this point more clearly, a schematic of the diffusion reaction process is shown in Fig. 5. At time t_1, at the A_nB/A interface, high-B A_nB (L_2 layer) reacts with A (L_3 layer) to form some new A_nB cells, leaving B vacancies (noted as V_Bs) in L_2 layer (time t_2). If bulk diffusivity is high, V_Bs simply diffuse through bulk (e.g., from L_2 to L_1, as shown by grey dotted arrows) to the B source. If bulk diffusion is frozen, the V_Bs diffuse first along A_nB/A inter-phase interface (as shown by green solid arrows), and then along A_nB grain boundaries to the B source. This process continues until this L_3 layer entirely becomes A_nB (time t_3), so the reaction frontier moves ahead to L_3/L_4, while the L_2/L_3 interface now becomes an inter-plane inside A_nB lattice. If bulk diffusion is frozen, the V_Bs in the L_2 layer that have not diffused to B source will be frozen in this layer forever, and will perhaps transform to A-on-B anti-site defects later (e.g., for Nb_3Sn, Nb-on-Sn anti-sites are more stable than Sn vacancies[24]). Since these point defects determine the A_nB composition, the X_B in this L_2 layer cannot change anymore regardless of μ_B variations in grain boundaries. That is to say, X_B of any point is just the X_{II} of the moment when the reaction frontier sweeps across this point, i.e., the $X_B(x)$ of an A_nB layer is simply an accumulation of X_{II}s with l increase. Returning to Fig. 3 (a), the dashed lines display the evolution of $X_B(x)$ with l increase for bulk diffusion, while that for grain boundary diffusion is shown by the solid lines. Since the energy dispersive spectroscopy (EDS) attached to scanning electron microscopes (SEM) that is used to measure the compositions typically has a spatial resolution of 0.5-2 μm, and thus mainly reflects the bulk composition, the composition characteristics of Nb_3Sn layers as described above can be explained. It should be noted that knowledge of the difference between

bulk diffusion and grain boundary diffusion is important in controlling the final composition of a compound. For instance, if bulk diffusivity is high, one method to form high-B A_nB is increasing the starting B/A ratio so that after long annealing time for homogenization subsequent to the full consumption of A, μ_B(M-B)=μ_B(A-X_u B). However, our experiments demonstrate that for compounds with low bulk diffusivity (e.g., Nb_3Sn), such an approach does not work; instead, controlling the X_{II}s while the compounds are growing is the only way. For those compounds with low but non-negligible bulk diffusivities, their compositions would be between these two extremes.

Then what determines the bulk composition as grain boundary diffusion dominates? From Fig. 5, it can be clearly seen that there is a competition deciding the V_B fraction in the frontier A_nB layer: at t_2 the reaction across the A_nB/A interface produces V_Bs in L_2 layer, while the diffusion of B along A_nB GBs and A_nB/A interface fills these V_Bs. Thus, if the diffusion rate is slow relative to the reaction rate at interface II (i.e., φ_{II} is low), a high fraction of V_Bs would be left behind as the interface II moves ahead, causing low B content; if, on the other hand, the diffusion rate is high relative to the reaction rate at interface II, the A_nB layer has enough time to get homogenized with the B source, causing low X_B gradient. In this case, the μ_B of B source and the reaction rate at interface I together set a upper limit for μ_B of A_nB.

Next, we will modify the above model for the case of grain boundary diffusion for quantitative analysis. As pointed out earlier, the chemical potentials of grain boundaries can change with μ_s and l, while those of the bulk cannot. In such a case, μ_I and μ_{II} (suppose the diffusivities along the inter-phase interfaces are large) can still be calculated using our model, provided that the $\mu(X)$ relation and D of the A_nB grain boundary (instead of the bulk) are used in all of the equations, and that φ_I and φ_{II} are multiplied by a factor of $\sum A_{GB}/A_{int}$ (where $\sum A_{GB}$ is the

sum of the cross section areas of the grain boundaries projected to the inter-phase interfaces), because B diffuses only along grain boundaries in A_nB while reactions occur at the entire interfaces. Approximately, $\sum A_{GB}/A_{int} \approx [1-d^2/(d+w)^2] \approx 2w/d$ (where w is the A_nB grain boundary width, and d is the grain size). Apparently, grain growth with annealing time reduces the diffusion rate. According to Eq. (8), a_{II} is determined by η and a_s, and increases with them, as shown by Fig. 6. Since $\eta=\varphi_{II}a_s/(\varphi_I a_s+\kappa l)= 1/[\varphi_I/\varphi_{II}+\kappa l/(\varphi_{II}a_s)]$, clearly η decreases as φ_I/φ_{II} and l increase, and the influence of l (which reflects the X_{II}-x gradient) is mitigated as $\varphi_{II}a_s$ increases. Thus, to improve X_{II} of A_nB at l=0, one should increase μ_s and the reaction rate at interface I, and reduce the reaction rate at interface II; meanwhile, to reduce $X_{II}(x)$ gradient, one should increase φ_{II} (which means improving the diffusion rate or reducing the reaction rate at interface II) and a_s. Apparently, these quantitative conclusions are consistent with the above qualitative analysis.

Next let us compare this model with the example of Nb_3Sn. It has been well established from experimental work that there are mainly two factors that can significantly influence the Sn content of Nb_3Sn in a Cu-Sn/Nb_3Sn/Nb diffusion reaction couple: heat treatment temperature and Cu-Sn source. The heat treatment temperature can simultaneously influence multiple factors of Eq. (8), such as a_s, D, and reaction rates at both interfaces, etc. Thus, the explanation of the influence of temperature on Sn contents using this theory requires knowledge of the quantitative variations of these factors with temperature. For the other factor, Cu-Sn source, the diffusion reaction couples can be classified into two types based on the Cu-Sn source: the type I uses bronze (with Sn content in Cu-Sn typically below 9 at.%) as Sn source, and the type II uses high-Sn Cu-Sn (e.g., Cu-25 at.% Sn). Previous measurements[4,8-10,25] show that both types of samples have Sn contents above 24 at.% for the Nb_3Sn layer next to the Cu-Sn source; however, they have distinct Sn content gradients as the Nb_3Sn layers grow thicker: the type I generally has Sn

content gradients above 3 at.%/μm[25], while those of the type II are below 0.5 at.%/μm[4,8-9]. Such a difference in the Sn content gradients leads to distinct grain morphologies and superconducting properties. The different X_{Sn} gradients in the two types of samples with different Cu-Sn sources can be easily explained by our theory above: according to Eq. (8), increased μ_s can decrease X_{Sn} gradients. It may also need further investigation regarding whether Cu-Sn source can also influence diffusion rates in Nb_3Sn layer (e.g., via thermodynamic factor), because greater D leads to greater φ_{II}, which helps decreasing X_{Sn} gradients. As to the phenomenon that different wires have similar X_{Sn} in the Nb_3Sn layer next to the Cu-Sn source, the relation between μ_{Sn}(Cu-Sn) and μ_{Sn}(Nb-X_{Sn} Sn) is required. The Cu-Sn system has been well studied, and the phase diagram calculated by the CALPHAD technique using the thermodynamic parameters given by Ref. 26 is well consistent with the experimentally measured diagram[27]. Thus, the parameters from Ref. 26 are used to calculate μ_{Sn} of Cu-Sn, which is shown in Fig. 7. On the other hand, although thermodynamic data of Nb-Sn system were proposed by Refs. 26 and 28, in these studies Nb_3Sn was treated as a line compound. However, some information about μ_{Sn} of Nb_3Sn can be inferred from its relation with μ_{Sn} of Cu-Sn: since Cu-7 at.% Sn leads to the formation of Nb-24 at.% Sn near the Cu-Sn source[25], we have μ_{Sn}(Cu-7 at.% Sn) ≥ μ_{Sn}(Nb-24 at.% Sn). Thus, the expected approximate μ_{Sn}(Nb-X_{Sn} Sn) curve in a power function is shown in Fig. 7. Besides, we can also infer that the Sn transfer rate at the Cu-Sn/Nb_3Sn interface must be much faster than that at the Nb_3Sn/Nb interface, so μ_{Sn} discontinuity across the interface I is small. These explain why low-Sn Cu-Sn can lead to the formation of high-Sn Nb_3Sn. It is worth mentioning that from Fig. 7, it is clear that the Taylor series for the true $a(X)$ relation of Nb_3Sn have more high-rank terms than $a(X) \approx a_l + \kappa(X-X_l)$; however, our numerical calculations show that adding high-rank terms to the $a(X)$ relation does not lead to different conclusions regarding the influences of a_s, φ_I, φ_{II}, and l on X_{II}. Thus, the above qualitative and quantitative analysis still applies.

In summary, a mathematical framework is developed to describe the compositions and layer growth rates of non-stoichiometric intermediate phases formed by diffusion reactions. The governing equations are derived and analytic solutions are given for compounds with narrow composition ranges under certain approximations. We also modify our model for compounds in which bulk diffusion is frozen, of which the bulk is not in equilibrium with the rest of the system. Based on this model, the factors that fundamentally determine the compositions of non-stoichiometric compounds formed by diffusion reactions are found and approaches to control the compositions are proposed.

Methods

For the Cu-Sn/Nb_3Sn/Nb diffusion reaction couples that were used for Sn content measurements (the results of which are shown in Fig. 4), the initial composition of the precursor Cu-Sn alloy was Cu-12 at.% Sn. The samples were reacted at 650 °C for 65 h, 130 h, 320 h, and 600 h. Then the samples were polished to 0.05 μm and the compositions were measured using an EDS system attached to an SEM. An accelerating voltage of 15 kV was used for the quantitative line scans. A standard Nb-25 at.% Sn bulk sample provided by Dr. Goldacker from Karlsruhe Institute of Technology was used for calibrating the Sn content of the samples. The standard deviation in the measurements was found to be about ± 0.5 at.%.

References

1. Kim, M., Baek, S., Paik, U., Nam, S. & Byun, J. Electrical conductivity and oxygen diffusion in nonstoichiometric TiO_{2-x}. *J. Korean Phys. Soc.* **32,** S1127-S1130 (1998).
2. Park, S. I., Tsuei, C. C. & Tu, K. N. Effect of oxygen deficiency on the normal and superconducting properties of $YBa_2Cu_3O_{7-\delta}$. *Phys. Rev. B* **37,** 2305-2308 (1988).

3. Noebe, R. D., Bowman, R. R. & Nathal, M. V. Physical and mechanical properties of the B2 compound NiAl. *Int. Mater. Rev.* **38,** 193-232 (1993).

4. Godeke, A. Performance boundaries in Nb_3Sn superconductors (Ph.D. thesis) 89-104 (University of Twente, 2005).

5. Xu, X., Sumption, M. D. & Peng, X. Internally oxidized Nb_3Sn strands with fine grain size and high critical current density. *Adv. Mater.* **27,** 1346-1350 (2015).

6. Charlesworth, J. P., Macphail, I. & Madsen, P. E. Experimental work on the niobium-tin constitution diagram and related studies. *J. Mater. Sci.* **5,** 580-603 (1970).

7. Zhou, J. *et al*. Evidence that the upper critical field of Nb_3Sn is independent of whether it is cubic or tetragonal. *Appl. Phys. Lett.* **99,** 122507 (2011).

8. Xu, X., Sumption, M. D. & Collings, E. W. Influence of heat treatment temperature and Ti doping on low-field flux jumping and stability in $(Nb\text{-}Ta)_3Sn$ strands. *Supercond. Sci. Technol.* **27**, 095009 (2014).

9. Peng, X. et al. Composition profiles and upper critical field measurement of internal-Sn and tube-type conductors. *IEEE Trans. Appl. Supercon.* **17,** 2668-2671 (2007).

10. Suenaga, M. in *Superconductor Materials Science: Metallurgy, Fabrication, and Applications* (eds Foner, S. & Schwartz, B. B.) 201-274 (Plenum, 1981).

11. Xu, X., Collings, E. W., Sumption, M. D., Kovacs, C. & Peng, X. The effects of Ti addition and high Cu/Sn ratio on tube type $(Nb, Ta)_3Sn$ strands, and a new type of strand designed to reduce unreacted Nb ratio. *IEEE Trans. Appl. Supercond.* **24,** 6000904 (2014).

12. Farrell, H. H., Gilmer, G. H. & Suenaga, M. J. Grain boundary diffusion and growth of intermetallic layers: Nb_3Sn. *J. Appl. Phys.* **45,** 4025-4035 (1974).

13. Gosele, U. & Tu, K. N. Growth kinetics of planar binary diffusion couples: "Thin-film case" versus "Bulk cases". *J. Appl. Phys.* **53,** 3252-3260 (1982).

14. Debkov, V. I. in *Reaction Diffusion and Solid State Chemical Kinetics* (ed. Debkov, V. I.) 3-19 (IPMS, 2002).

15. Gusak, A. M. *et al*. in *Diffusion-controlled Solid State Reactions: In Alloys, Thin Films and Nanosystems* (eds Gusak, A. M. *et al*.) 99-133 (Wiley-VCH, 2010).

16. Tu, K. N. & Gusak, A. M. in *Kinetics in Nanoscale Materials* (eds Tu, K. N. & Gusak, A. M.) 187-193 (Wiley-VCH, 2014).

17. Kodentsov, A. A., Bastin, G. F. & van Loo, F. J. J. The diffusion couple technique in phase diagram determination. *J. Alloy Compd.* **320,** 207-217 (2001).

18. Gong, W., Zhang, L., Wei, H. & Zhou, C. Phase equilibria, diffusion growth and diffusivities in Ni-Al-Pt system using Pt/β-NiAl diffusion couples. *Prog. Nat. Sci.* **21,** 221-226 (2011).

19. Sandim, M. J. R. *et al*. Grain boundary segregation in a bronze-route Nb_3Sn superconducting wire studied by atom probe tomography. *Supercond. Sci. Technol.* **26,** 055008 (2013).

20. Laurila, T., Vuorinen, V., Kumar, A. K. & Paul, A. Diffusion and growth mechanism of Nb_3Sn superconductor grown by bronze technique. *Appl. Phys. Lett.* **96,** 231910 (2010).

21. Cui, Z. W., Gao, F. & Qu, J. M. Interface-reaction controlled diffusion in binary solids with applications to lithiation of silicon in lithium-ion batteries. *J. Mech. Phys. Solids.* **61,** 293-310 (2013).

22. Bochvar, A. A. *et al*. Diffusion of tin during growth of the Nb_3Sn layer. *Met. Sci. Heat. Treat.* **22,** 904-907 (1980).

23. Müller, H. & Schneider, Th. Heat treatment of Nb_3Sn conductors. *Cryogenics* **48,** 323-330 (2008).

24. Besson, R., Guyot, S. & Legris, A. Atomic-scale study of diffusion in A15 Nb_3Sn. *Phys. Rev. B* **75,** 054105 (2007).

25. Abächerli, V. *et al*. The influence of Ti doping methods on the high field performance of $(Nb, Ta, Ti)_3Sn$ multifilamentary wires using Osprey bronze. *IEEE Trans. Appl. Supercon.* **15,** 3482-3485 (2005).

26. Li, M., Du, Z., Guo, C. & Li, C. Thermodynamic optimization of the Cu-Sn and Cu-Nb-Sn systems. *J. Alloys Compd.* **477,** 104-117 (2009).

27. Hansen, M. & Anderko, R. P. in *Constitution of binary alloys* (eds Hansen, M. & Anderko, R. P.) 634 (McGraw-Hill, 1958).

28. Toffolon, C., Servant, C., Gachon, J. C. & Sundman, B. Reassessment of the Nb-Sn system. *J. Phase Equilib.* **23,** 134-139 (2002).

Acknowledgements

The authors thank S. Dregia and J. Morral for useful discussions, and X. Peng and Hyper Tech Research Inc. for providing Nb_3Sn samples for analysis. The work is funded by the US Department of Energy, Division of High Energy Physics, under an SBIR program.

Author Contributions

X.X initiated this study, developed the model, and wrote the manuscript. M.D.S. supported this work, discussed the results, and reviewed the manuscript.

Additional information:

Competing Financial Interests: The authors declare no competing financial interests.

Figure Captions

FIG. 1: Schematic of an isothermal cross section of the M-A-B ternary phase diagram. The shaded region shows the equilibria among M-X_1 B, A-X_1 B, and A phases, and the dashed line shows the equilibrium between M-B and A_nB phases.

FIG. 2: (a) Schematic of the M-B/A_nB/A diffusion reaction system in the planar geometry, and (b) X_B profiles of the system.

FIG. 3: (a) The calculated $X_B(x)$ profiles of the hypothetical system for the analytic and numerical solutions, with and without the assumption that $X_B(x)$ is linear, respectively. (b) The $l(t)$ results from the numerical calculations, with the fits of $l=q[\sqrt{(t+\tau)}-\sqrt{\tau}]$ and $l=bt^m$.

FIG. 4: The measured X_{Sn}s of a Cu-Sn/Nb_3Sn/Nb system after various annealing times at 650°C. The standard deviation in the Sn content measurements is around ± 0.5 at.%.

FIG. 5: A schematic of the diffusion reaction process for grain boundary diffusion.

FIG. 6: The variation of a_{II} with η and a_s, according to Eq. (8).

FIG. 7: The variation of μ_{Sn} with X_{Sn} for Cu-Sn calculated based on thermodynamic data given in Ref. 26, and a rough, speculative $\mu_{Sn}(X_{Sn})$ relation for Nb_3Sn sketched according to the phase formation relation between Cu-Sn and Nb_3Sn.

FIG 1

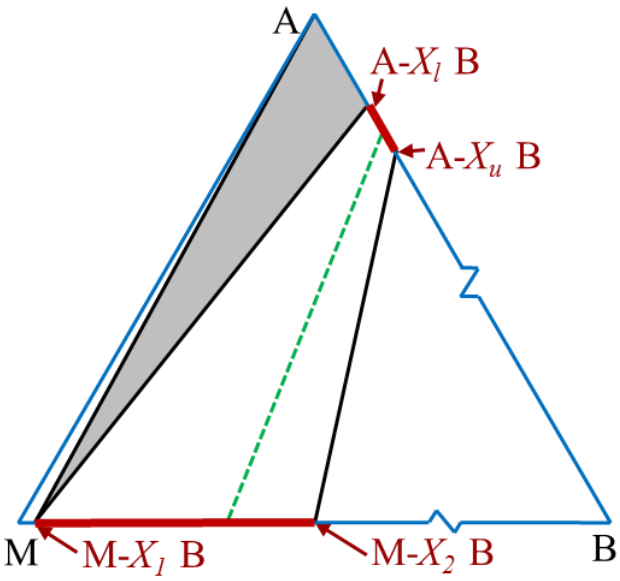

FIG 2

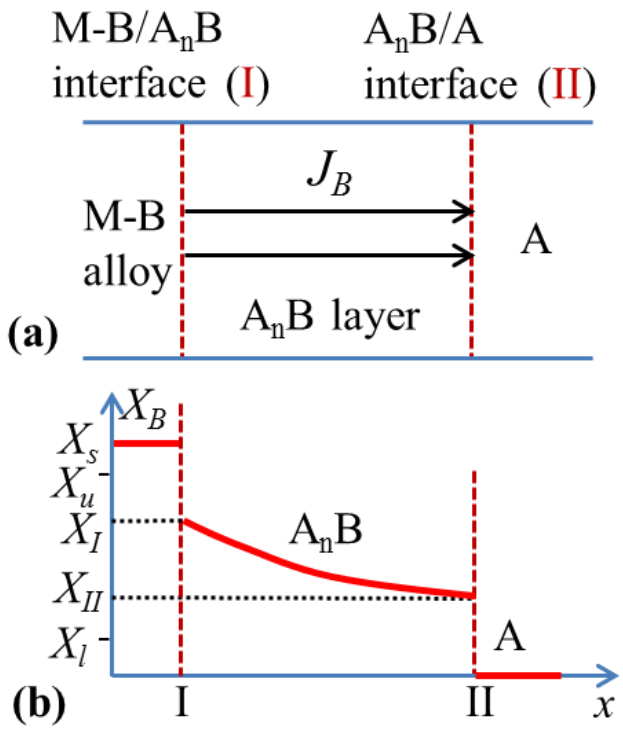
M-B/AnB
interface (I)
AnB/A
interface (II)
JB
M-B
alloy
A
AnB layer
(a)
XB
Xs
Xu
XI
XII
Xl
AnB
A
(b)
I
II
x

Xu *et al.*

FIG 3

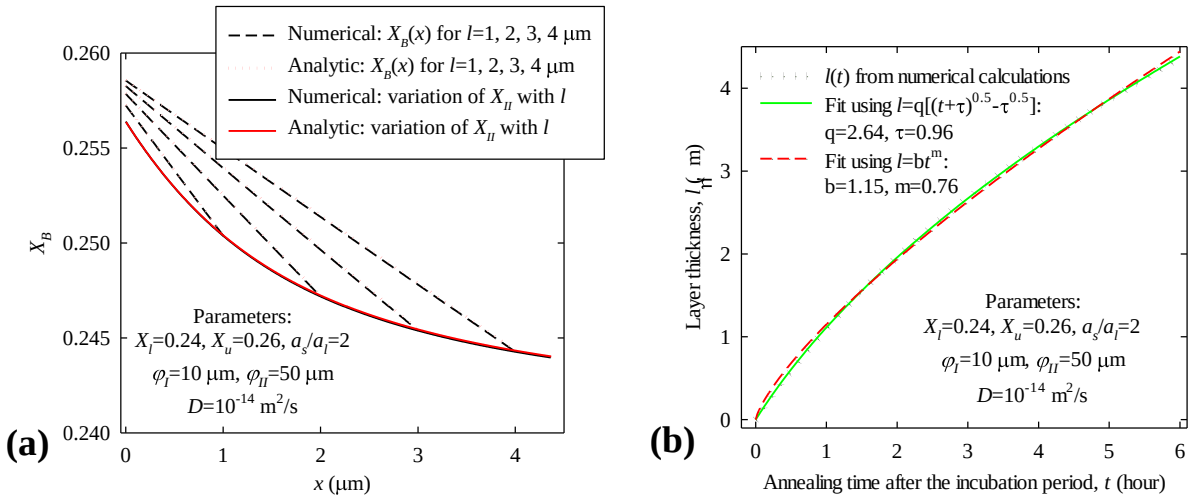
Numerical: $X_B(x)$ for l=1, 2, 3, 4 μm
Analytic: $X_B(x)$ for l=1, 2, 3, 4 μm
Numerical: variation of X_{II} with l
Analytic: variation of X_{II} with l
Parameters:
X_l=0.24, X_u=0.26, a_s/a_l=2
φ_I=10 μm, φ_{II}=50 μm
D=10^{-14} m^2/s
X_B
x (μm)
(a)
$l(t)$ from numerical calculations
Fit using l=q[(t+τ)$^{0.5}$-τ$^{0.5}$]:
q=2.64, τ=0.96
Fit using l=bt^m:
b=1.15, m=0.76
Layer thickness, l (μm)
Annealing time after the incubation period, t (hour)
(b)

FIG 4

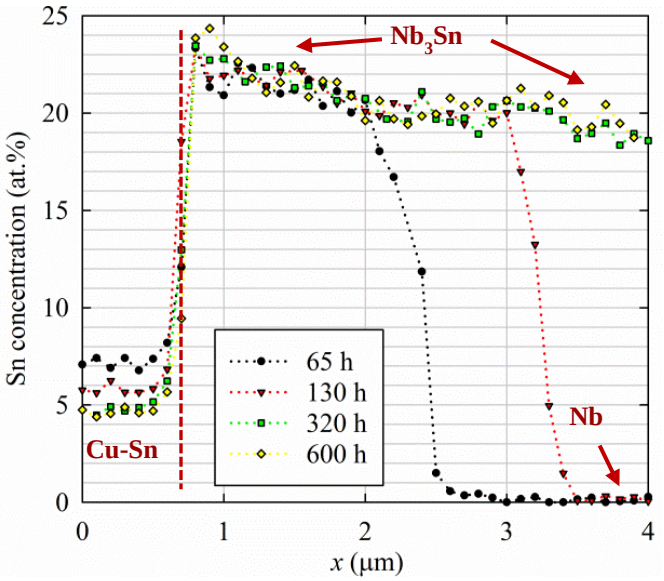
Nb3Sn
Nb
Cu-Sn
65 h
130 h
320 h
600 h
Sn concentration (at.%)
x (μm)
0
5
10
15
20
25
0
1
2
3
4

Xu *et al.*

FIG 5

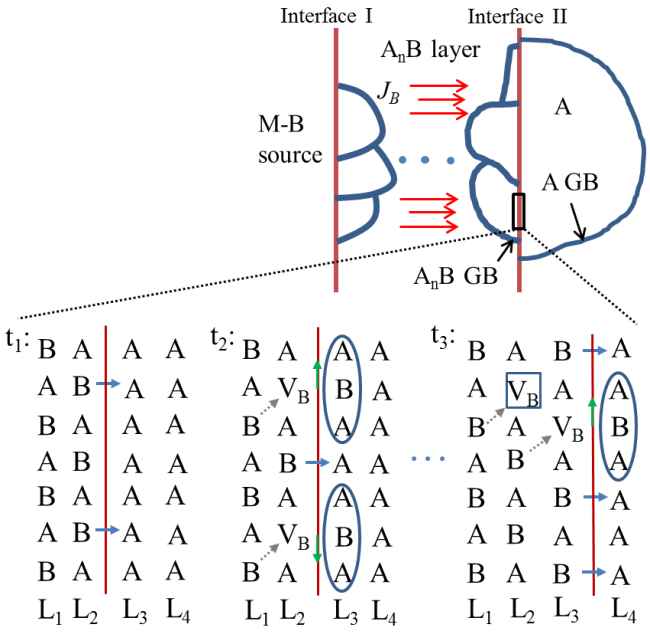
Interface I
Interface II
A_nB layer
J_B
M-B source
A
A GB
A_nB GB
t_1:
t_2:
t_3:
V_B
L_1 L_2 L_3 L_4

FIG 6

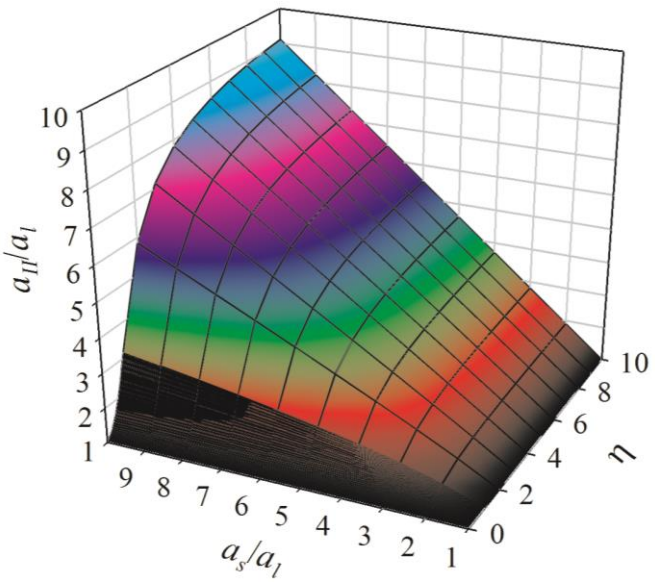

Xu *et al.*

FIG 7

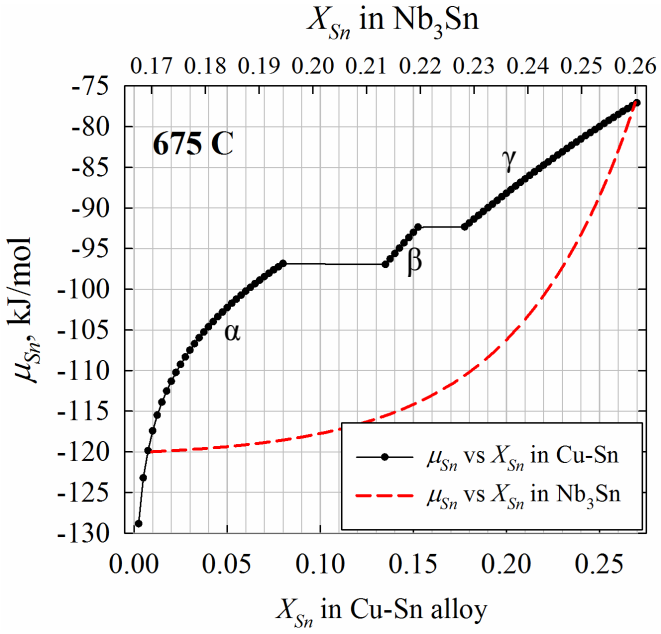
X_{Sn} in Nb_3Sn
0.17 0.18 0.19 0.20 0.21 0.22 0.23 0.24 0.25 0.26
675 C
α
β
γ
μ_{Sn}, kJ/mol
-75 -80 -85 -90 -95 -100 -105 -110 -115 -120 -125 -130
μ_{Sn} vs X_{Sn} in Cu-Sn
μ_{Sn} vs X_{Sn} in Nb_3Sn
0.00 0.05 0.10 0.15 0.20 0.25
X_{Sn} in Cu-Sn alloy